Journal of The Electrochemical Society, **155** (11) A798-A805 (2008)
0013-4651/2008/155(11)/A798/8/$23.00 © The Electrochemical Society

Capacitive Behavior of Porous Nickel Oxide/Hydroxide Electrodes with Interconnected Nanoflakes Synthesized by Anodic Electrodeposition

Mao-Sung Wu,*,z Yu-An Huang, and Chung-Hsien Yang

Department of Chemical and Materials Engineering, National Kaohsiung University of Applied Sciences, Kaohsiung 807, Taiwan

Nanostructured nickel hydroxides are galvanostatically deposited onto a stainless steel substrate by a plating bath of nickel sulfate, sodium acetate, and sodium sulfate at room temperature. The anodically deposited nickel hydroxide electrodes are highly porous and composed of interconnected nanoflakes about 12–16 nm in thickness. Pore size of the deposited electrode increases with decreasing the depositing current density. X-ray diffraction patterns show that the deposited nickel hydroxide converts into nickel oxide at annealing temperature above 300°C. Annealing temperature influences both the electrical resistance and the grain size of the electrode and, consequently, determines the capacitive behavior of the electrode investigated by cyclic voltammetry in 1 M KOH aqueous solution. An optimal annealing temperature of 300°C is obtained in terms of the electrode's specific capacitance. An electrode with larger pores deposited at lower current density has a higher specific capacitance because larger pores facilitate the ion diffusion rate. An electrode with smaller pore size deposited at higher current density exhibits more kinetically reversible behaviors, resulting in a better high-rate capability.
 [DOI: 10.1149/1.2969948]

Manuscript submitted March 20, 2008; revised manuscript received July 21, 2008. Published September 5, 2008.

Electrochemical capacitors are energy-storage devices that have attracted much attention due to their high power capability and long cycle life compared to traditional batteries.[1] Due to an increasing demand of high-power devices such as portable electronic devices and electric vehicles, electrochemical capacitors have been studied extensively in recent years. Generally, to have a single battery of both high power density and high energy density is a tremendous challenge;[2] therefore, a hybrid system connecting an electrochemical capacitor of high power density to a battery of high energy density in parallel provides a solution.

There are two major types of electrochemical capacitors categorized by the charge-storage mechanism, the electric double-layer capacitor (EDLC) and the electrochemical capacitor (supercapacitor). EDLC stores energy in electric double layers at the electrode/electrolyte interface. Electrochemical capacitors utilize both electrical double-layer and interfacial redox processes (electrochemical faradaic reactions between electrode materials and ions) to store energy in the appropriate potential window. It is believed that the specific capacitance of the electric double layer on a flat electrode surface is small because of the much smaller electroactive surface area compared to a porous electrode. Using a porous electrode with a higher specific surface area may increase the specific capacitance of an EDLC; consequently, carbon materials with a high specific surface area have been chosen as electrode materials for EDLC.[3] However, the major problem of high-specific-surface-area carbon is that not all the Brunauer–Emmett–Teller (BET) surface area is electrochemically accessible when in contact with an electrolyte solution.[4]

For the past decade, several research teams have focused on the development of alternative materials for electrochemical capacitors; the aim was to achieve fast reversible faradaic reactions, in which the charge-storage mechanism is based predominantly on pseudocapacitance.[5] Some transition metal oxides such as ruthenium oxides, manganese oxides, cobalt oxides, and nickel oxides/hydroxides have met the qualifications. Among these transition metal oxides, a hydrous form of ruthenium oxide in aqueous H_2SO_4 possesses a high specific capacitance of 720 F g^{-1} and excellent cycle-life stability.[6,7] Although the performance is excellent, ruthenium oxide is too expensive for commercialization. Therefore, attention is focused on alternative electrode materials that are inexpensive and exhibit capacitive behavior similar to that of ruthenium oxide.

Nickel oxide is a promising candidate for electrochemical capacitor materials. Many preparation methods have been explored to fabricate nickel oxides to achieve the requirements. Techniques such as chemical precipitation,[8] reactive radio-frequency sputtering,[9] calcining,[10] electrochemical cathodic deposition,[11-17] and electrochemical anodic deposition[18,19] have been proposed. Among these synthetic methods, the electrochemical deposition technique has one advantage over the others: the weight and thickness of the film may be easily controlled by adjusting the current, bath composition, and bath temperature.[11,20] In addition, an electrode composed of nanoparticles is more difficult to fabricate by the traditional slurry-coating method, because nanoparticles have poor dispersibility in slurry (composed of solvent, nanoparticles, polymer binder, conducting agent, etc.). Thus, it is more advantageous to have an electrode of nanostructured nickel oxide fabricated by electrochemical deposition which deposits the active material directly onto the substrate at room temperature without templates.

Nanostructured materials are important in electrochemical capacitors because they have a high specific surface area, fast redox reactions, and a shortened diffusion path in the solid phase; the capacitive behavior is, therefore, enhanced by the material's nanostructure. Most of the synthesized nickel oxides for electrochemical capacitors are nanopowders. More recently, nanowhiskers or small nanowires fabricated by templates have been alternative structures.[10,18] In electrochemical preparation of nickel oxide/hydroxide, electrochemically cathodic deposition in nitrate-based bath is generally used to fabricate film electrodes,[11-16] but electrochemically anodic deposition is rarely studied.

The cathodic deposition process is based on the reduction of nitrate to ammonium ion and OH^- ion. The production of OH^- ions increases the local pH near the electrode; the nickel ions then react with the OH^- ions to form insoluble nickel hydroxides at the surface. However, of some concern in this process is that the nickel ions may be reduced and deposited in the metallic state within the pores of the deposited nickel hydroxide film.[21] The presence of metallic nickel would presumably exclude active material (nickel hydroxide) from the electrode.[21] The anodic deposition is based on the oxidation of Ni^{2+} ions to Ni^{3+} ions, and then the Ni^{3+} ions react with the OH^- ions to form insoluble nickel oxide/hydroxide deposits on the electrode.[22] Therefore, anodic deposition can avoid the codeposition of metallic nickel into nickel hydroxide/oxide matrix. In addition, most of the cathodically deposited nickel oxides/hydroxides

* Electrochemical Society Active Member.
z E-mail: ms_wu@url.com.tw

for electrochemical capacitors are nanoparticles. Previous results showed that the anodically deposited nickel oxide is composed of nanoflakes.[19,23] By tuning the deposition parameters, it is possible to prepare nickel oxide/hydroxide films with various morphologies and structures. Therefore, in this work, the anodic deposition is used to fabricate nanostructured nickel oxide/hydroxide films having interconnected nanoflakes by a plating bath of sodium acetate, nickel sulfate, and sodium sulfate at room temperature without templates. In addition, the electrochemical performance of the deposited electrodes is analyzed.

Experimental

Nickel oxide/hydroxide electrodes were electrochemically prepared on both sides of stainless steel (SS) foils (2×2 cm) by applying three anodic currents of 0.05, 0.25, and 0.5 mA cm^{-2}, respectively, in a solution bath of 0.13 M sodium acetate, 0.13 M nickel sulfate, and 0.1 M sodium sulfate at room temperature.[22,24] Prior to deposition, SS foils were polished with emery paper and rinsed by ultrasonic vibrations in acetone and deionized (DI) water, respectively. The plating solution was vigorously stirred by a Teflon stir on a magnetic hot plate during deposition. After deposition, the resultant brown-colored films were rinsed several times in DI water and dried at 100, 200, 300, 400, and 500°C, respectively, for 1 h in air. The amount of nickel oxide/hydroxide deposits was measured by a microbalance (Ohaus G160, USA) with an accuracy of 0.01 mg and was kept almost the same (about 0.5 mg) for each electrode by adjusting the deposition time. All experiments were carried out in a beaker-type electrochemical cell equipped with the working electrode, a platinum counter electrode, and a saturated Ag/AgCl reference electrode. The geometric surface area of a platinum counter electrode was 2×2 cm.

Surface morphology of the deposited nickel oxide/hydroxide electrodes was examined by scanning electron microscopy (SEM, Hitachi S4700-I, Japan) with an accelerating voltage of 5 keV. The crystal structure of the deposited electrodes was identified by a glance-angle X-ray diffractometer (XRD, Rigaku D/MAX2500, Japan) with a Cu Kα target (wavelength = 1.54056 Å) and an incidence angle of 2°. Diffraction data were collected for 1 s at each 0.05° step width over 2θ, ranging from 20 to 80°.

For electrical-resistance measurements, each electrode was placed between two commercial brass pistons. The diameter of the two cylindrical brasses was 10 mm. A constant force was applied in the direction perpendicular to the electrode surface for determining the electrical resistance of electrodes. Four-probe impedance measurements were carried out in a computer-controlled potentiostat/galvanostat (CH Instruments CHI 608, USA) at room temperature. Measurements were done on the electrode of the synthesized nickel oxide/hydroxide in the frequency range from 1 to 10^5 Hz under open-circuit conditions at a perturbation amplitude of 10 mV. The resistances were deduced from the intercept of the arc with the real Z' axis in the Nyquist plots.[25]

Capacitive behavior of the deposited electrodes was determined by cyclic voltammetry (CV) in a three-electrode cell (beaker-type electrochemical cell) with 1 M KOH aqueous solution. According to the previous researches,[11-14] the potential was cycled at a scan rate of 25 mV s^{-1} using a potentiostat (CH Instruments CHI 608, USA) in the potential range of −0.2 to 0.45 V vs a saturated Ag/AgCl reference electrode. In order to obtain the effect of scan rate on the capacitive behavior of the electrode, the potential was cycled at different scan rates. Charge/discharge and cycle-life stability were performed by a potentiostat (Princeton Applied Research EG&G 362, USA) in the potential range of −0.2 to 0.45 V vs Ag/AgCl at different charge/discharge currents. All data-acquisition functions in EG&G 362 were carried out through an interface card (Labjack U12, USA) with LabVIEW software. The ac impedance measurements were conducted by means of a potentiostat (CH Instruments CHI 608, USA) under open-circuit conditions. The equivalent circuit fitting of the ac impedance data was done using Zview, the electrochemical software from Scribner. An ac perturbation amplitude of 10 mV vs the open-circuit potential was applied in the frequency range between 50 kHz and 0.1 Hz.

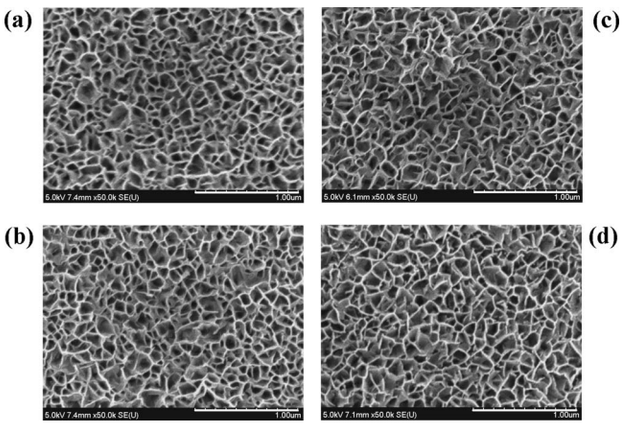

Figure 1. SEM micrograph of the electrochemically deposited nickel oxide/hydroxide electrode annealed at (a) 100, (b) 200, (c) 300, and (d) 500°C for 1 h in air. The electrode was deposited at a current density of 0.25 mA cm^{-2}.

Results and Discussion

Figure 1 shows the surface morphology of deposited nickel oxide/hydroxide electrodes after heat-treatments. The morphology is not greatly affected by the annealing temperature ranging from 100 to 500°C. Surface morphology of the deposited electrodes is highly porous and composed of interconnected nanoflakes. Nanoflakes distributed on the SS substrate are about 12–16 nm in thickness, roughly estimated from SEM image. Electrodes having thinner nanoflakes may shorten the solid-state diffusion path for the hydroxyl ions. In addition, it is generally recognized that a highly porous structure may provide a large surface area for electrolyte access;[26] therefore, porous nickel oxide/hydroxide electrode with interconnected nanoflakes may benefit from its capacitive behavior. Specific surface area of the chemical precipitated nickel oxide/hydroxide is usually measured by means of the BET technique using nitrogen gas to relate the capacitance of the material.[25] Generally, in order to obtain a reliable BET result, a minimum amount of material of about 200 mg is needed. However, in this work, it is difficult to deposit electrochemically the requisite quantity of material needed for BET analysis, because the amount of deposits is about 0.5 mg for each electrode. However, a large surface area of electrode materials does not always guarantee high specific capacitance when used in aqueous or nonaqueous electrochemical capacitors, because not all BET surface area is electrochemically accessible when immersed in electrolyte.

In addition to the surface morphology, the crystal structure is identified by a XRD. Figure 2 shows the XRD patterns of the SS substrate and the deposited nickel oxide/hydroxide electrodes after annealing at various temperatures. Except for the diffraction peaks of the SS substrate, the XRD pattern of the electrode after 100°C annealing resembles nickel hydroxide hydrate (JCPDS 22-0444). As the annealing temperature is higher than 200°C, in addition to the diffraction peaks of the SS substrate, some diffraction peaks of nickel oxide hydroxide appear (JCPDS 47-1179). As the annealing temperature is higher than 300°C, in addition to a characteristic diffraction peak of the nickel oxide hydroxide (101) and the diffraction peaks of the SS substrate, the XRD patterns of 300, 400, and 500°C closely resemble that of cubic NiO (nickel oxide, JCPDS 47-1049). The change in crystallinity after annealing at higher temperatures may be attributed to the removal of both the water of hydration and the absorbed water from the solid phase of nickel hydroxide structure, whereupon the nickel hydroxide phase is converted into nickel oxide phase.[14,27] In addition, water content within

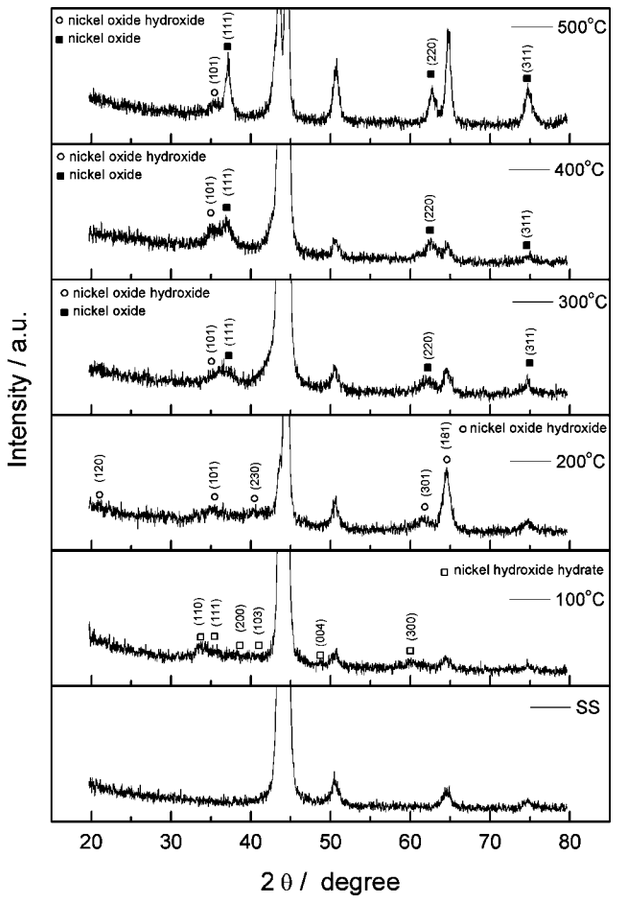

Figure 2. XRD patterns of the SS substrate and the deposited nickel oxide/hydroxide electrodes annealed at different temperatures. The electrode was deposited at a current density of 0.25 mA cm^{-2}.

nickel oxide/hydroxide is known to affect the electrochemical reactivity and the thermodynamic stability of nickel oxide.[12]

Furthermore, the XRD peak at about $2\theta = 37.2°$ becomes broader as the annealing temperature decreases from 500 to 300°C; such a widening peak indicates a poor crystallinity and a decrease in the average grain size. The mean grain size of the deposited nickel oxide/hydroxide is calculated using Scherrer's equation, $D = 0.9\lambda/(\beta \cos \theta)$, where λ is the X-ray wavelength (1.54056 Å), β is the full width at half-maximum, and θ is the Bragg angle. Figure 3 shows the calculated grain size of the nickel oxide/hydroxide associated with annealing temperature. The higher the annealing temperature, the larger the grain size. It is believed that a poorly crystalline-structured NiO has a larger surface area than that of a highly crystalline-structured NiO because NiO in a poorly crystalline-structured form has a much smaller grain size.[24]

Annealing temperature affects not only the grain size of the deposited nickel oxide/hydroxide but also the electrical resistance, as shown in Fig. 3. Electrical resistance of the electrode decreases with elevating the annealing temperature in the range between 100 and 300°C, reaches a minimum at 300°C, then increases with further increase in the annealing temperature. The deposited electrodes of annealing temperature lower than 300°C (nickel hydroxide) have high electrical resistance, probably because nickel hydroxide is an intrinsically poor electrical conductor.[25] The deposited electrodes of annealing temperatures higher than 300°C have increasing resistance as the annealing temperature increases. According to Comnellis et al.,[27] heat-treatment of nickel oxide in the vicinity of 300°C gives a nonstoichiometric nickel oxide, which has a high conductivity. However, above that range, nickel oxide (n-type semiconductor) becomes insulating and is unable to store charges or to react electrochemical and faradaically.[27]

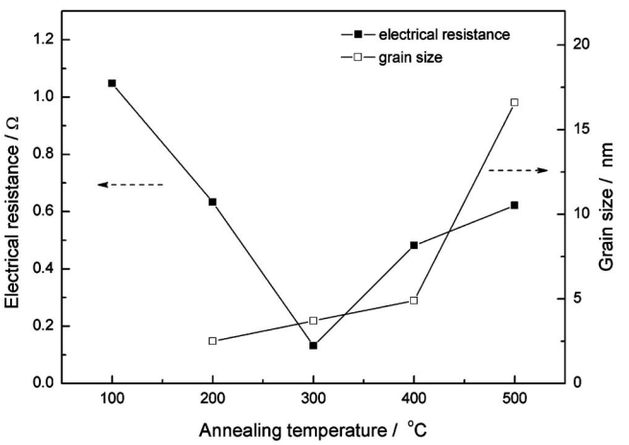

Figure 3. Effects of annealing temperature on the electrical resistance and grain size of the deposited nickel oxide/hydroxide electrode. The electrode was deposited at a current density of 0.25 mA cm^{-2}.

CV is generally used to characterize the capacitive behavior of an electrode material. An ideal electrical double-layer capacitor of flat electrode has a current response in cyclic voltammogram shapes, such as a rectangular mirror image, with respect to the zero-current line; the cyclic voltammogram also shows a rapid current response at each reversal potential end.[1,28] Generally, the electrical double-layer capacitance is independent of the scan rate and the applied potential.[1] When the faradaic reaction and ohmic resistance resulted from electrolyte diffusion within the porous electrode are involved in the cyclic voltammogram, a rectangular mirror image cannot be maintained.[1] Figure 4 shows the cyclic voltammograms of the deposited nickel oxide electrodes after annealing at various temperatures at a scan rate of 25 mV s^{-1}. The cyclic voltammograms presented in Fig. 4 are relative to the first scan cycle. Clearly, the capacitive behavior of the nickel oxide/hydroxide electrode is considerably affected by the annealing temperature. Among these cyclic voltammograms, an electrode after annealing at 300°C has redox peaks and shows the highest current response. The redox peaks appear only in the nickel oxide/hydroxide film heated at 300°C, indicating that the nickel oxide/hydroxide film after annealing at 300°C

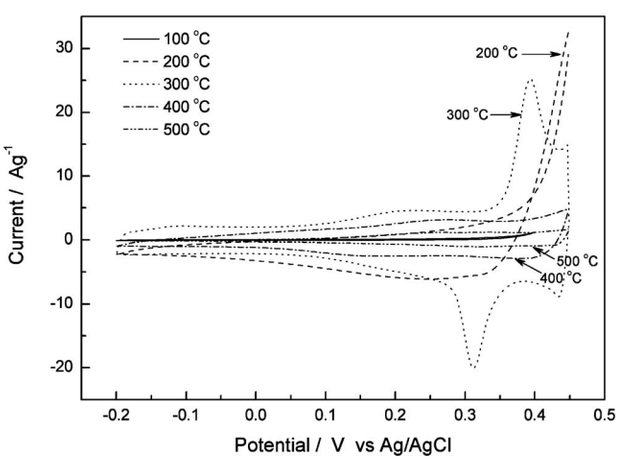

Figure 4. Cyclic voltammograms of the deposited nickel oxide/hydroxide electrodes annealed at different temperatures at a scan rate of 25 mV s^{-1}. The electrode was deposited at a current density of 0.25 mA cm^{-2}.

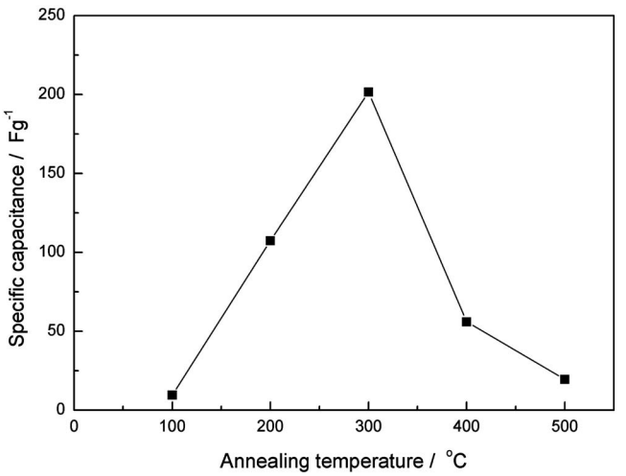

Figure 5. Specific capacitances of the deposited nickel oxide/hydroxide electrodes annealed at different temperatures at a CV scan rate of 25 mV s^{-1}. The electrode was deposited at a current density of 0.25 mA cm^{-2}.

exhibits a larger electroactive area for redox reactions compared with that annealed at other temperatures. The electroactive area of the materials is generally affected not only by the effective surface area for electrolyte accessibility but also by the electrical conductivity for electron transfer. The capacitance of nickel oxide capacitor in alkaline solution comes from charge storage in the electric double layer at the electrode/electrolyte interface and charge storage in the host material through redox reactions on the surface and hydroxyl ion diffusion in the host material. Through redox reactions (faradaic reactions), much higher capacitance can be stored in a redox capacitor than in a double-layer capacitor. The redox couple of nickel oxide electrodes in alkaline solution is as follows[16,29,30]

$$\mathrm{NiO} + \mathrm{OH}^- \leftrightarrow \mathrm{NiOOH} + \mathrm{e}^- \qquad [1]$$

The cyclic voltammogram of a blank SS substrate after 300°C heating for 1 h in 1 M KOH aqueous solution (not shown here) was scanned at a scan rate of 25 mV s^{-1} for comparison, and the specific capacitance (less than 0.01 F g^{-1}) is small compared with that of deposited nickel oxide (about 200 F g^{-1}) after 300°C annealing. Therefore, capacitance mainly comes from the nickel oxide deposits instead of the SS substrate.

Specific capacitance of the deposited electrodes can be calculated from the cyclic voltammograms according to the following equation

$$C = \frac{1}{\nu \cdot w \cdot \Delta V} \int_{V_i}^{V_f} i dV \qquad [2]$$

where C is the specific capacitance of nickel oxide/hydroxide electrode (F g^{-1}), w is the mass of nickel oxide/hydroxide (g), ν is the scan rate (V s^{-1}), i is the cathodic or anodic current (A) in the potential range of V_i to V_f, and ΔV is the applied potential window (V). Figure 5 shows the specific capacitance of deposited electrode associated with the annealing temperature. Obviously, the specific capacitance is sensitive to the annealing temperature; an optimal specific capacitance of about 202 F g^{-1} is obtained for an electrode after annealing at 300°C. The specific capacitance value increases initially with annealing temperature, reaches a maximum at the annealing temperature of 300°C, and then decreases with further increase in annealing temperature. The variation trend of the specific capacitance is similar to that of electrical conductivity (the inverse of electrical resistance illustrated in Fig. 3). Referring to Fig. 3, there is an increase trend in the electrical resistance and the grain size when the annealing temperature exceeds 300°C. These results suggest that the grain size (or specific surface area) and the electrical resistance are essential to maximize the capacitance values. The high capacitance of the nickel oxide/hydroxide electrode after annealing at 300°C may be attributed to the low electrical resistance (high electrical conductivity) and high surface area (small grain size) providing a large electroactive area for redox reactions and charge storage. The total electroactive sites on the surface of the materials are strongly affected not only by the specific surface area (grain size) for electrolyte accessibility but also by the electrical conductivity for electron transfer.

Usually, the specific surface area of the electrode materials is measured by means of the BET technique using nitrogen gas to relate the capacitance of the materials. However, as mentioned above, it is difficult to deposit electrochemically the requisite quantity of material needed for BET analysis in this work. Instead, we use the ac impedance technique to explain the effect of annealing temperature on capacitance. Figure 6 shows the Nyquist plots of the deposited nickel oxide/hydroxide electrodes after annealing at various temperatures. The corresponding equivalent circuit for impedance analysis is displayed in the inset of Fig. 6. At high frequencies, the intercept at real part (Z') is a combinational resistance of ionic resistance of electrolyte, intrinsic resistance of substrate, and contact resistance at the active material/current collector interface (R_e).[31] This value is almost the same for all electrodes. A major difference is the semicircle in the high-frequency range, which corresponds to the charge-transfer resistance (R_{ct}) caused by the faradaic reactions and the double-layer capacitance (C_{dl}) on the grain surface. Charge separation at micropores is represented by the transmission line Z_p which relates to the distributed electronic and ionic conductivity and double-layer capacitance inside the micropores; C_{lc} is the limit capacitance.[32] The calculated charge-transfer resistances for the deposited electrodes after annealing at 100, 200, 300, 400, and 500°C are 2100, 6, 2, 340, and 5000 Ω, respectively. The higher the charge-transfer resistance, the lower the specific capacitance of the electrode. The charge-transfer resistance decreases initially with annealing temperature, reaches a minimum at 300°C, then increases with further increase in annealing temperature. The deposited nickel oxide/hydroxide electrode annealing at 300°C has the lowest charge-transfer resistance reflecting the highest specific capacitance. The charge-transfer resistance is related to the electroactive surface area (the combination of electrolyte accessible area and electrical conductivity) of the electrode materials. The larger the electroactive surface area, the lower the charge-transfer resistance.[33] Although a poorly crystalline-structured nickel hydroxide electrode after annealing at 100°C has smaller grain sizes, providing a larger surface area, its electrical conductivity is low. It is concluded that increasing the annealing temperature enhances the electrical conductivity because charge-transfer resistance is reduced in the temperature range of 100–300°C. This relationship is responsible for a low capacitance for 100°C annealing. When the annealing temperature rises over 300°C, the specific capacitance is decreased with increasing annealing temperature; this may result from the decreased specific surface area (increased grain size) and the decreased electrical conductivity (increased electrical resistance) by the annealing temperature.

Another appreciable difference in the Nyquist plots is the straight line in the low-frequency range. An ideally polarizable capacitance gives rise to a straight vertical line along the imaginary axis (Z''). The deposited nickel oxide/hydroxide electrodes after annealing at 100 and 500°C have no polarizable capacitance corresponding to the result of specific capacitance in Fig. 5. For a real circuit of a capacitor and a resistance in series, the Nyquist plot in the low-frequency range definitely shows a finite slope, which corresponds to a capacitor's diffusive resistance of electrolyte in electrode pores and the hydroxyl ion diffusion in host materials. The value of the slope is in the series 300 > 200 > 400°C. An increased slope of the diffusion line is attributed to the lowered diffusion resistance by the shortened diffusion path for hydroxyl ions.

Figure 7 shows the galvanostatic charge/discharge curve of a deposited nickel oxide/hydroxide electrode after annealing at 300°C for 1 h. The charge and discharge current densities were set at a

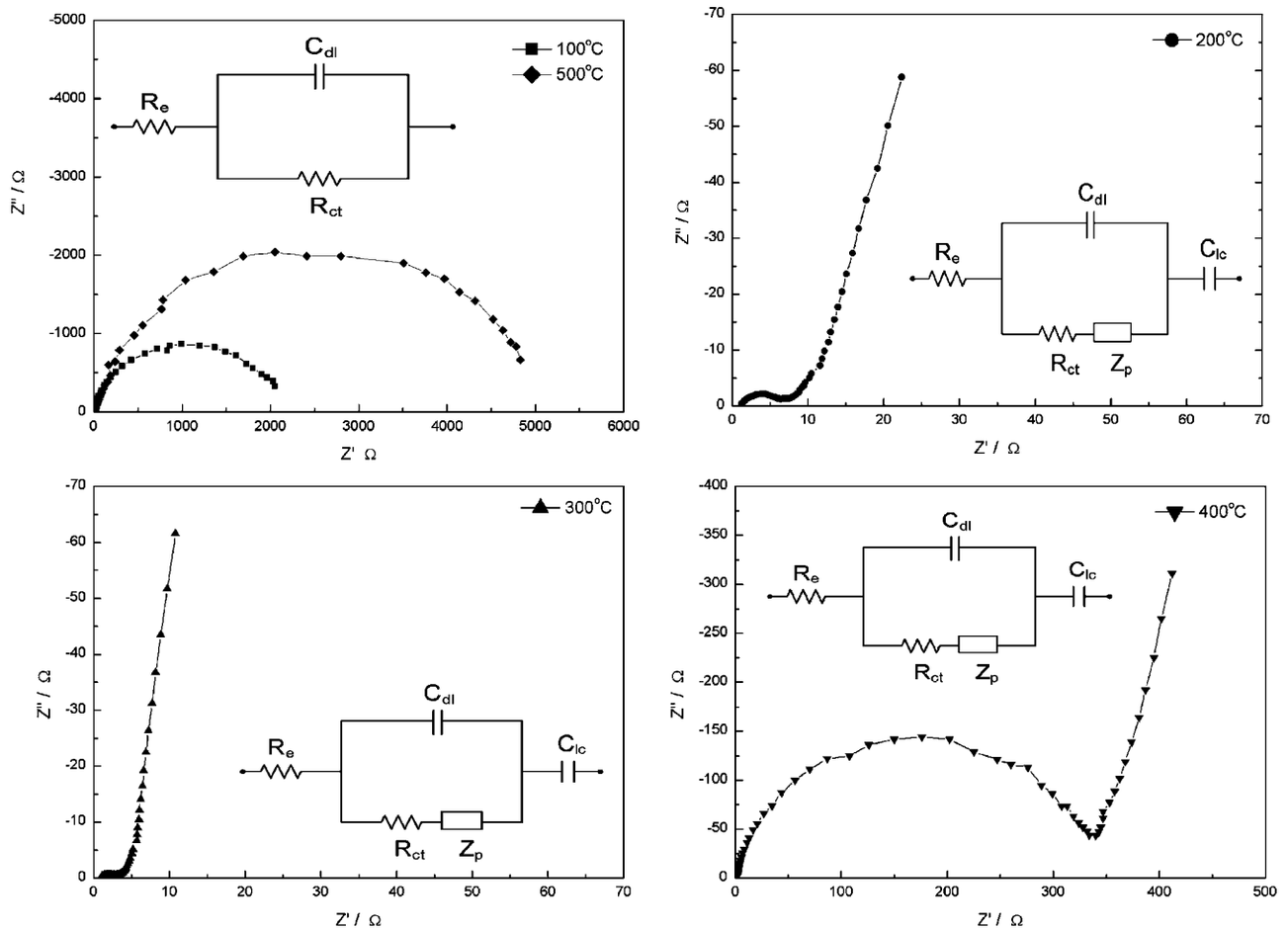

Figure 6. Nyquist plots of the deposited nickel oxide/hydroxide electrodes annealed at different temperatures. The electrode was deposited at a current density of 0.25 mA cm^{-2}.

constant current density of 2 A g^{-1}. Total time for charging (from −0.2 to 0.45 V) and discharging (from 0.45 to − 0.2 V) processes are almost the same. Similar time length implies a high reversibility of the faradaic reaction on the surface of nickel oxide grains, which agrees with the CV results. The specific capacitance of an electrode during galvanostatic charge/discharge can also be calculated by the following equation[34,35]

$$C = \frac{i \cdot \Delta t}{w \Delta V} \qquad [3]$$

where w is the mass of nickel oxide (g), ΔV is the potential window (V), and i is the discharge current (A) applied for time Δt (s). Specific capacitance of the deposited electrode after annealing at 300°C is about 215 F g^{-1} at 2 A g^{-1} charge/discharge, which is close to the measured capacitance of 202 F g^{-1} by CV at a scan rate of 25 mV s^{-1}.

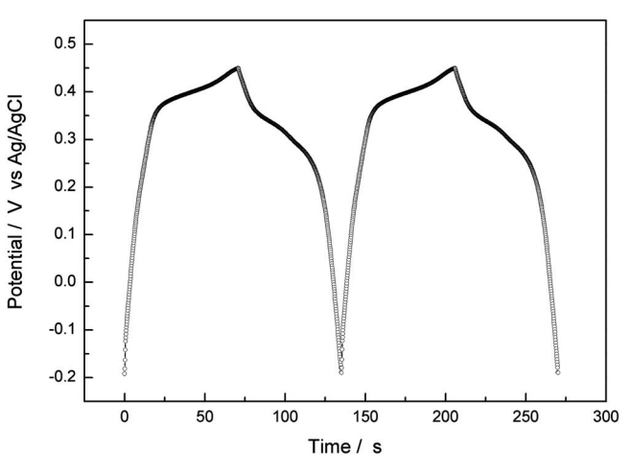

Figure 7. Galvanostatic charge/discharge curve of a deposited nickel oxide/hydroxide electrode annealed at 300°C. The electrode was deposited at a current density of 0.25 mA cm^{-2}. The charge and discharge currents were set at 2 A g^{-1}.

Figure 8 shows the SEM micrographs of the nickel oxide/hydroxide electrodes deposited at 0.05 and 0.5 mA cm^{-2} and annealed at 100 and 500°C. In comparison with an electrode deposited at 0.25 mA cm^{-2} after annealing at 100 and 500°C (Fig. 1a and d), surface morphology of the deposited electrode is slightly affected by the annealing temperature but apparently affected by the depositing current density. Nanoflakes deposited at a high current density of 0.5 mA cm^{-2} are denser than those deposited at a low current density of 0.05 mA cm^{-2}, indicating that pore size of the electrode deposited at low current density is larger than that of the electrode deposited at high current density. Figure 9 shows the cyclic voltammograms of the electrodes deposited at various current densities after annealing at 300°C for 1 h. Clearly, the depositing current density affects the capacitive behavior of the deposited nickel oxide

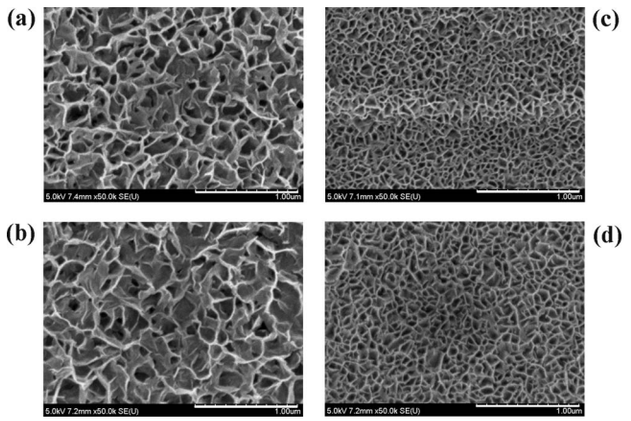

Figure 8. SEM micrograph of the nickel oxide/hydroxide electrode deposited at 0.05 mA cm^{-2} after annealing at (a) 100 and (b) 500°C and deposited at 0.5 mA cm^{-2} after annealing at (c) 100 and (d) 500°C.

electrode. During CV scan, the corresponding current of the electrode deposited at 0.05 mA cm^{-2} is much higher than that of the electrode deposited at 0.5 mA cm^{-2}. According to Eq. 2, the specific capacitance of the electrode deposited at low current density is, therefore, higher than that of the electrode deposited at high current density. Possibly, the microtextural character of an electrode influences greatly the electrochemical performance. Among these electrodes, an electrode deposited at low current density has a higher capacitance because the larger pores facilitate the ion-diffusion rate.

The ability to charge and discharge at high current is a crucial characteristic for capacitors because of the high power demand from portable electronic power tools and electric vehicles. From Eq. 2 and 3, the specific capacitance of the deposited electrodes can be calculated by means of the CV method and the galvanostatic charge/discharge method. A high scan rate in CV corresponds to the high current in charge/discharge and vice versa. Generally, a specific capacitance is decreased with an increasing scan rate and charge/discharge current. Liu et al.[8] pointed out that due to the limiting space in a porous electrode, a diffuse layer may not be developed. Thus, the total charge stored in the microporous electrodes of a double-layer capacitor is limited by the capability of the capacitor to develop a diffuse layer in micropores. An electrochemical capacitor not only stores energy as a double-layer capacitor, but it also exhibits electrochemical faradaic reactions between electrode materials and ions in the appropriate potential window. Therefore, during high-rate charging and discharging, the specific capacitance of an electrochemical capacitor is dominated by both the diffusive resistance of electrolyte in electrode pores and the reaction resistance on the surface of active materials. Figure 10 shows the specific capacitances of electrodes deposited at 0.05, 0.25, and 0.5 mA cm^{-2} at various scan rates. Prior to measurement, the electrodes were annealed at 300°C for 1 h. Clearly, all electrodes have higher specific capacitance at low scan rate than those at high scan rate. An electrode deposited at 0.05 mA cm^{-2} has a specific capacitance as high as 260 F g^{-1} at a scan rate of 10 mV s^{-1}, and the value reduces to 177 F g^{-1} (68% capacitance of 10 mV s^{-1}) at a scan rate of 100 mV s^{-1}. The nickel oxide electrode deposited at 0.05 mA cm^{-2} shows a higher specific capacitance compared with that deposited at 0.5 and 0.25 mA cm^{-2} even at a high scan rate of 100 mV s^{-1}, because electrode deposited at 0.05 mA cm^{-2} has larger pores in the nickel oxide layer and allows for easier electrolyte penetration.

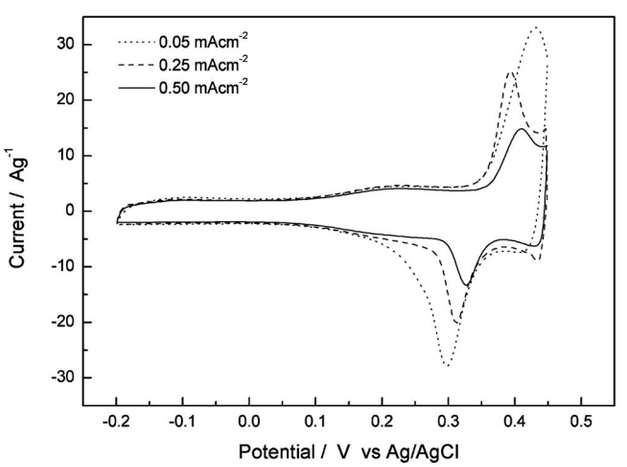

Figure 9. Cyclic voltammograms of the nickel oxide/hydroxide electrodes deposited at various current densities after annealing at 300°C for 1 h. The CV scan rate was set at 25 mV s^{-1}.

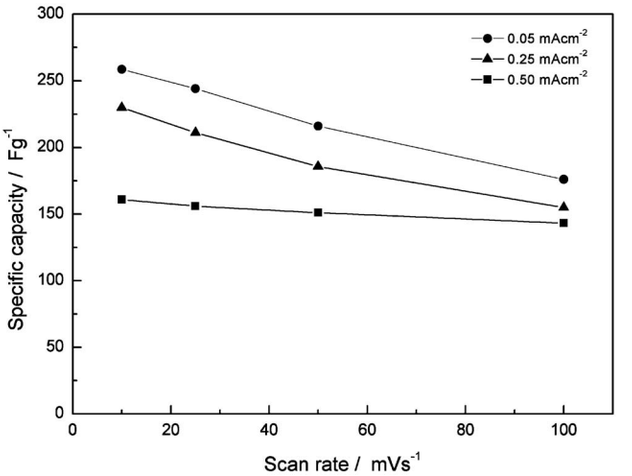

Figure 10. Specific capacitances of the nickel oxide/hydroxide electrodes deposited at 0.05, 0.25, and 0.5 mA cm^{-2} at various scan rates. Prior to measurement, the electrodes were annealed at 300°C for 1 h.

It was reported that if the electrode is well wetted and is charging and discharging at a sufficiently low rate to retain thermodynamic equilibrium, the micropore (>0.5 nm) surface area of the electrode measured from N_2 gas adsorption should be accessed by the ions and thus contribute to the total double-layer capacitance.[36] If the micropores are inaccessible to aqueous electrolyte, leaving only the external surface area of the electrode available, then consequently the double-layer capacitance will be unrealistically high.[36] Pore diameters of the nickel oxide deposited at 0.5 mA cm^{-2} are in the range of 50–100 nm, and these values are large enough for the penetration of the electrolyte. However, in addition to the penetration of the electrolyte within pores, the diffusion rate of ions within pores should be taken into account, which may be a limiting step during high-rate charging and discharging.[37] It is generally believed that capacitors are operated at high-rate charging and discharging. Therefore, the pore size in this work may be a critical factor affecting the capacitive behavior of the deposited nickel oxide/hydroxide films at the same annealing temperature of 300°C.

Compared to the redox peak feature of the nickel oxide electrode deposited at 0.05 mA cm^{-2} (larger pore size), the redox peak feature in CVs for the electrode deposited at 0.25 or 0.5 mA cm^{-2} (smaller pore size) shows more kinetically reversible behaviors (Fig. 9). As evident from Fig. 9, the nickel oxide electrode with smaller pore size deposited at 0.25 or 0.5 mA cm^{-2} shows smaller redox peak potential separation in the CVs than that of NiO with larger pore size deposited at 0.05 mA cm^{-2}. In addition, as shown in Fig. 10,

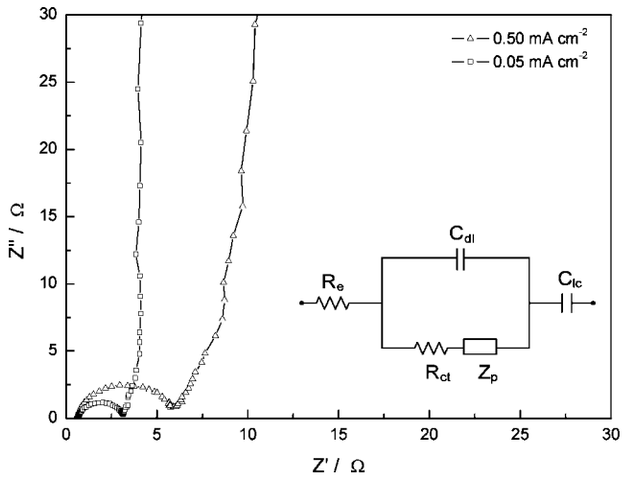

Figure 11. Nyquist plots of the nickel oxide/hydroxide electrodes deposited at 0.05 and 0.5 mA cm^{-2} after annealing at 300°C for 1 h.

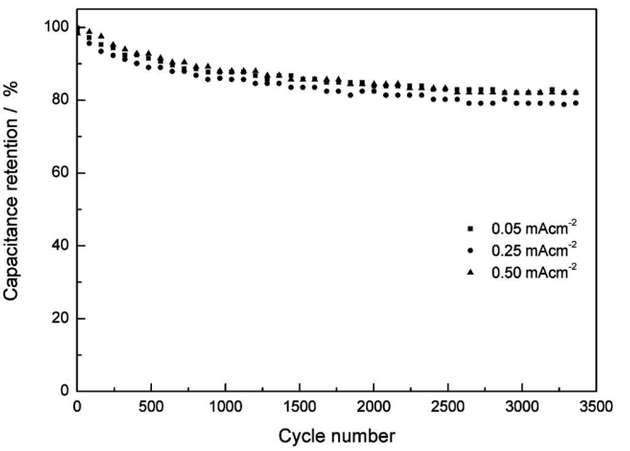

Figure 12. Relationship between capacitance retention and cycle number of the nickel oxide/hydroxide electrodes deposited at various current densities after annealing at 300°C for 1 h.

the nickel oxide electrode with smaller pore size shows a much superior high-rate capability than NiO with larger pore size. For example, when a scan rate increases from 10 to 100 mV s^{-1}, NiO deposited at 0.05 mA cm^{-2} (larger pore size) shows about 32% loss of capacitance, whereas NiO deposited at 0.5 mA cm^{-2} (smaller pore size) shows less than 10% loss of capacitance. Therefore, in terms of the high-rate capability (power density), NiO with smaller pore size shows a better performance than NiO with larger pore size.

Compared with previous literatures, a specific capacitance of 260 F g^{-1} of nickel oxide electrode at a CV scan rate of 10 mV s^{-1} is much higher than that obtained from chemical precipitation.[25] Liu et al.[8] have reported an electrochemical capacitor using nickel oxide prepared by the chemical precipitation method; a specific capacitance of 65 F g^{-1} was obtained. A less expensive, more controllable electrochemical method of preparing porous nickel oxide capacitors was reported by Srinivasan et al.; a specific capacitance of 59 F g^{-1} based on a device fabricated from two identical nickel oxide electrodes was obtained at a slow scan rate of 20 mV s^{-1}.[11] Recently, a higher specific capacitance of nickel oxide has been reported. Nanoarrays with ordered mesoporous structure (capacitance of 120 F g^{-1}) were synthesized by calcining nickel nitrate at 550°C within a silica template;[10] three-dimensional nanowhiskers prepared by potentiodynamically depositing nickel hydroxide (nickel chloride plating bath) on SS and heating in air at 300°C for 3 h has a capacitance of 138 F g^{-1}.[18] A high specific capacitance of 194 F g^{-1} was reported for the activated-carbon material loaded with nickel oxide.[38]

Figure 11 shows the Nyquist plots of the electrodes deposited at 0.05 and 0.5 mA cm^{-2}. The corresponding equivalent circuit for impedance analysis is displayed in the inset of Fig. 11. A major difference in the Nyquist plots is the semicircle in the high-frequency range, which corresponds to the charge-transfer resistance and is associated with the surface properties of porous electrode. Obviously, the charge-transfer resistance of electrode deposited at 0.05 mA cm^{-2} is lower than that deposited at 0.5 mA cm^{-2}. This finding suggests that electrode deposited at low current density (0.05 mA cm^{-2}) provides a larger electroactive area for charge storage and electrochemical reaction due to an improvement in diffusion rate of ions within the larger pores.

Based on the analysis above, in comparison with other annealing temperatures, the deposited nickel oxide/hydroxide after annealing at 300°C is suitable for electrochemical capacitor use because it has the highest specific capacitance. When considering the practical use of an electrochemical capacitor, cycle-life stability is also important. Figure 12 shows the relationship between capacitance retention (discharge) and cycle number of the electrodes deposited at various current densities after annealing at 300°C. Cycle-life stability is carried out by galvanostatic charge/discharge cycling at 2 A g^{-1}. Clearly, depositing current density has little influence on the cycle-life stability. Capacitance retention of the electrodes decays appreciably at the beginning of charge/discharge test cycles; however, it stabilizes and degrades greatly after 1000 test cycles. Capacitance retention of the electrodes after 3500 cycles is about 80%. The deposited nickel oxide/hydroxide electrodes after annealing at 300°C show stable capacitance retention during cycling and have high stability for long-time capacitor applications in KOH aqueous solution.

Conclusion

Surface morphology of the nickel oxide/hydroxide electrodes deposited by electrochemically anodic deposition is highly porous and composed of interconnected nanoflakes of thickness 12–16 nm. Annealing temperature, in the range of 100–500°C, has little influence on the surface morphology. However, annealing temperature influences not only the grain size but also the electrical resistance of deposited nickel oxide/hydroxide electrode and consequently determines the capacitor behavior. Nickel hydroxide is changed to nickel oxide by increasing the annealing temperature over 300°C. CVs of the electrodes after annealing at different temperatures are investigated in the potential range from −0.2 to 0.45 V vs Ag/AgCl in 1 M KOH aqueous electrolyte. The deposited electrode after annealing at 300°C shows the lowest electrical resistance and consequently exhibits the highest specific capacitance. With an annealing temperature below 300°C, the electrode has a smaller grain size, providing a larger surface area, but the electrical resistance of the electrode is high; poor capacitive behavior comes mainly from the electrical resistance. When the annealing temperature rises over 300°C, the specific capacitance is decreased with increasing the annealing temperature; this may result from the decreased specific surface area (increased grain size) and the decreased electrical conductivity (increased electrical resistance) by annealing temperature. Depositing current density influences pore size of the porous nickel oxide/hydroxide electrode; the higher the current density, the smaller the pore size. An electrode deposited at a low current density of 0.05 mA cm^{-2} shows a higher capacitance compared with that deposited at 0.5 and 0.25 mA cm^{-2} even at high CV scan rates, because electrode deposited at 0.05 mA cm^{-2} has larger pores in the nickel oxide layer, making electrolyte penetration easier. However, nickel oxide electrode with smaller pore size, which exhibits more kinetically reversible behaviors, shows a better high-rate capability (power density) than nickel oxide electrode with larger pore size.

The effect of depositing current density on the cycle-life stability of electrode is negligible. Capacitance retention of the electrodes deposited at various current densities decays appreciably at the beginning of charge/discharge test cycles; however, it stabilizes and degrades greatly after 1000 test cycles. With a high capacitance and a stable cycle-life performance, the nickel oxide electrode deposited at 0.05 mA cm^{-2} after annealing at 300°C is a promising candidate for electrochemical capacitor materials.

Acknowledgment

The authors gratefully acknowledge financial support from the National Science Council, Taiwan, Republic of China (project no. NSC 96-2221-E-151-027).

National Kaohsiung University of Applied Sciences assisted in meeting the publication costs of this article.

References

1. B. E. Conway, *J. Electrochem. Soc.*, **138**, 1539 (1991).
2. M. S. Wu, C. Y. Lin, Y. Y. Wang, C. C. Wan, and C. R. Yang, *Electrochim. Acta*, **52**, 1349 (2006).
3. E. Frackowiak and F. Béguinm, *Carbon*, **39**, 937 (2001).
4. D. Qu, *J. Power Sources*, **109**, 403 (2002).
5. S. Sarangapani, B. V. Tilak, and C. P. Chen, *J. Electrochem. Soc.*, **143**, 3791 (1996).
6. J. P. Zheng and T. R. Jow, *J. Electrochem. Soc.*, **142**, L6 (1995).
7. J. P. Zheng, P. J. Cygan, and T. R. Jow, *J. Electrochem. Soc.*, **142**, 2699 (1995).
8. K. C. Liu and M. A. Anderson, *J. Electrochem. Soc.*, **143**, 124 (1996).
9. S. H. Lee, C. E. Tracy, and J. R. Pitts, *Electrochem. Solid-State Lett.*, **7**, A299 (2004).
10. Y. G. Wang and Y. Y. Xia, *Electrochim. Acta*, **51**, 3223 (2006).
11. V. Srinivasan and J. W. Weidner, *J. Electrochem. Soc.*, **144**, L210 (1997).
12. V. Srinivasan and J. W. Weidner, *J. Electrochem. Soc.*, **147**, 880 (2000).
13. E. E. Kalu, T. T. Nwoga, V. Srinivasan, and J. W. Weidner, *J. Power Sources*, **92**, 163 (2001).
14. K. W. Nam and K. B. Kim, *J. Electrochem. Soc.*, **149**, A346 (2002).
15. K. W. Nam, W. S. Yoon, and K. B. Kim, *Electrochim. Acta*, **47**, 3201 (2002).
16. K. W. Nam, E. S. Lee, J. H. Kim, Y. H. Lee, and K. B. Kim, *J. Electrochem. Soc.*, **152**, A2123 (2005).
17. D. D. Zhao, M. W. Xu, W. J. Zhou, J. Zhang, and H. L. Li, *Electrochim. Acta*, **53**, 2699 (2008).
18. K. R. Prasad and N. Miura, *Appl. Phys. Lett.*, **85**, 4199 (2004).
19. M. S. Wu, Y. A. Huang, C. H. Yang, and J. J. Jow, *Int. J. Hydrogen Energy*, **32**, 4153 (2007).
20. M. S. Wu, P. C. Chiang, J. T. Lee, and J. C. Lin, *J. Phys. Chem. B*, **109**, 23279 (2005).
21. D. F. Pickett and J. T. Maloy, *J. Electrochem. Soc.*, **125**, 1026 (1978).
22. D. Tench and L. F. Warren, *J. Electrochem. Soc.*, **130**, 869 (1983).
23. M. S. Wu, Y. A. Huang, J. J. Jow, W. D. Yang, C. Y. Hsieh, and H. M. Tsai, *Int. J. Hydrogen Energy*, **33**, 2921 (2008).
24. M. S. Wu and C. H. Yang, *Appl. Phys. Lett.*, **91**, 033109 (2007).
25. M. S. Wu and H. H. Hsieh, *Electrochim. Acta*, **53**, 3427 (2008).
26. R. N. Reddy and R. G. Reddy, *J. Power Sources*, **156**, 700 (2006).
27. C. H. Comnellis and I. A. Groza, *Thermochim. Acta*, **136**, 19 (1988).
28. H. Y. Lee and J. B. Goodenough, *J. Solid State Chem.*, **144**, 220 (1999).
29. C. Natarajan, H. Matsumoto, and G. Nogami, *J. Electrochem. Soc.*, **144**, 121 (1997).
30. P. Delichere, S. Joiret, A. Hugot-Le Goff, K. Bange, and B. Hetz, *J. Electrochem. Soc.*, **135**, 1856 (1988).
31. J. Gamby, P. L. Taberna, P. Simon, J. F. Fauvarque, and M. Chesneau, *J. Power Sources*, **101**, 109 (2001).
32. A. D. Fabio, A. Giorgi, M. Mastragostino, and F. Soavi, *J. Electrochem. Soc.*, **148**, A845 (2001).
33. M. S. Wu, *Appl. Phys. Lett.*, **87**, 153102 (2005).
34. M. Ramani, B. S. Haran, R. E. White, and B. N. Popov, *J. Electrochem. Soc.*, **148**, A374 (2001).
35. A. W. Goldenstein, W. Rostoker, W. Schossberger, and G. Gutzeit, *J. Electrochem. Soc.*, **104**, 104 (1957).
36. H. Shi, *Electrochim. Acta*, **41**, 1633 (1996).
37. M. S. Wu, T. L. Liao, Y. Y. Wang, and C. C. Wan, *J. Appl. Electrochem.* **34**, 797 (2004).
38. G. H. Yuan, Z. H. Jiang, A. Aramata, and Y. Z. Gao, *Carbon*, **43**, 2913 (2005).